Antiviral Research 95 (2012) 93–103

Contents lists available at SciVerse ScienceDirect

Antiviral Research

journal homepage: www.elsevier.com/locate/antiviral

Understanding the molecular mechanism of sequence dependent Tenofovir removal by HIV-1 reverse transcriptase: Differences in primer binding site versus polypurine tract

Pinar Iyidogan, Karen S. Anderson *

Department of Pharmacology, Yale University School of Medicine, New Haven, CT 06520, USA

ARTICLE INFO

Article history:
Received 28 April 2012
Revised 17 May 2012
Accepted 18 May 2012
Available online 1 June 2012

Keywords:
Human immunodeficiency virus type 1
Reverse transcriptase
Antiretroviral agents
Nucleoside reverse transcriptase inhibitor
Tenofovir

ABSTRACT

Tenofovir (TFV) is a nucleotide reverse transcriptase inhibitor (NtRTI) that is often administered as first-line therapy against human immunodeficiency virus type-1 (HIV-1) infection and acts as a chain terminator when incorporated into viral DNA. However, HIV-1 reverse transcriptase (RT) excises TFV in the presence of either ATP or pyrophosphate, which is an important drug resistance mechanism that would interfere with the effective treatment. Previous studies have shown conflicting results on excision efficiencies for TFV-terminated primer-templates derived from either primer binding site (PBS) or polypurine tract (PPT) sequences. To provide mechanistic insight into the variation in TFV removal from both sequences that are vital for the HIV-1 life cycle, we compared the efficiencies of removal reaction in response to sequence dependence via utilizing blocked PBS and PPT primer-templates. We found an enhanced TFV excision with PPT sequence over PBS sequence through ATP-mediated removal and a subsequent incorporation of ATP into the unblocked primers. Furthermore, the rate of pyrophosphorolytic excision of TFV from PPT sequence was 21-fold higher than that for the PBS sequence. However, the addition of efavirenz, nonnucleoside reverse transcriptase inhibitor (NNRTI), to the removal reaction effectively inhibits the TFV excision from both primers by forming a stable complex that would leave TFV inaccessible for excision. These results illuminate the degree of primer-template sequence contribution on TFV removal as well as increase our understanding of the molecular mechanism for the beneficial effects of widely used combinations of antiretroviral regimens in the context of synergistic antiviral activity and drug resistance.

1. Introduction

Developing a cure for HIV-1 infection still remains to be a major challenge, however combination therapy also known as highly active antiretroviral therapy (HAART) has been proven more effective in reducing viral load and delaying the emergence of resistance mutations than monotherapy (single-drug therapy) (Hammer et al., 1994; De Clercq, 2010). HAART generally combines three antiretroviral drugs in a daily regimen. The most common antiretroviral drug combination given as a first-line therapy consists of two nucleoside/nucleotide reverse transcriptase inhibitors (NRTIs/NtRTIs)[1] and a nonnucleoside reverse transcriptase inhibitor (NNRTI) (De Clercq, 2009). NRTIs and NtRTIs are prodrugs that require metabolic activation through cellular phosphorylation to their triphosphate and diphosphate derivatives, respectively. These derivatives serve as alternative substrates for the viral DNA synthesis catalyzed by HIV-1 RT while competing with the natural substrates, deoxyribonucleoside triphosphates (dNTPs), in order to terminate viral DNA chain extension upon their incorporation (De Clercq and Neyts, 2009). A common resistance mechanism that HIV-1 exploits against N[t]RTIs is phosphorolysis representing the reversal of the polymerization reaction in order to restore the DNA synthesis. In this mechanism, RT utilizes ATP or inorganic pyrophosphate (PP_i) as a co-substrate to remove the incorporated nucleoside analog monophosphate (NA-MP) that terminates the DNA elongation (Arion et al., 1998; Meyer et al., 1998, 1999). NNRTIs are allosteric inhibitors that

Abbreviations: HIV-1, human immunodeficiency virus type 1; WT RT, wild type reverse transcriptase; N[t]RTI, nucleoside [nucleotide] reverse transcriptase inhibitor; TFV, tenofovir; NNRTI, nonnucleoside reverse transcriptase inhibitor; EFV, efavirenz; PPT, polypurine tract; PBS, primer binding site; dNTP, deoxynucleoside triphosphate; ATP, adenosine triphosphate; PP_i, inorganic pyrophosphate.

* Corresponding author. Address: Department of Pharmacology, Yale University School of Medicine, 333 Cedar Street, SHM B-350B, P.O. Box 208066, New Haven, CT 06520-8066, USA. Tel.: +1 203 785 4526; fax: +1 203 785 7670.
E-mail address: karen.anderson@yale.edu (K.S. Anderson).

[1] NRTI and NtRTI are interchangeably used and indicated as N[t]RTI throughout the text.

0166-3542/$ - see front matter © 2012 Elsevier B.V. All rights reserved.
http://dx.doi.org/10.1016/j.antiviral.2012.05.012

bind to the RT at a hydrophobic pocket ~10 Å away from the polymerase active site in the palm subdomain of p66 (Tantillo et al., 1994; Das et al., 2005, 2012). These structurally diverse molecules are noncompetitive inhibitors with respect to dNTPs and have no direct effect on nucleic acid binding to RT (Spence et al., 1995; Zhan et al., 2009). Earlier work has showed that the various combinations of N[t]RTIs and NNRTIs exhibit synergistic effects on the inhibition of viral replication in cell culture as well as in patients in the clinical setting (Staszewski et al., 1999; De Clercq, 2009; Tsibris and Hirsch, 2010).

The FDA recently approved a single tablet (Atripla) fixed dose combination regimen that consists of tenofovir disoproxil fumarate (TDF), emtricitabine (FTC), and efavirenz (EFV) for the treatment of HIV-1 infection due to its promising viral suppression in clinic (FDA, 2009; Killingley and Pozniak, 2007). In the Atripla coformulation, tenofovir (TFV), the parent drug of TDF, ((*R*-9-[2-(phosphonomethoxypropyl)adenine])) is an NtRTI with an acyclic moiety instead of deoxyribose sugar ring that links the adenosine base to a phosphonate group that replaces the α-phosphate portion of the triphosphate form of nucleotides in addition to FTC ((−)-β-2′,3′-dideoxy-5-fluoro-3′-thiacytidine), which is an NRTI along with EFV ((4*S*)-6-chloro-4-(2-cyclopropylethynyl)-4-(trifluoromethyl)-2,4-dihydro-1*H*-3,1-benzoxazin-2-one) as an NNRTI. The chemical structures of TFV, FTC and EFV are shown in Fig. 1. Recently, Feng et al. reported a mechanistic study on the additive and synergistic antiviral activities of this triple combination as their findings demonstrated that EFV promotes a stable complex that resembles the dead-end-complex (DEC) formation while inhibiting the removal of incorporated TFV or FTC-monophosphate (FTC-MP) from primer terminus (Feng et al., 2009). The current study further probes the components of Atripla combination by studying the molecular mechanism for EFV and TFV synergy, which complements our previous report (Basavapathruni et al., 2004) on the antiviral synergy mechanism between FTC and EFV using ATP-mediated removal assay.

Previous biochemical studies on the phosphorolytical removal of TFV reported controversial results using the standard enzymatic experimental approaches. While an inefficient ATP-mediated TFV excision was reported using the HIV-1 genomic PBS sequence for the TFV terminated DNA:DNA primer/template (P/T) (Naeger et al., 2001; Boyer et al., 2004), another study demonstrated a highly efficient ATP-dependent TFV removal from a DNA:DNA P/T containing the HIV-1 specific PPT sequence catalyzed by WT and mutant RT (Marchand et al., 2007). Both PPT sequence and the aforementioned PBS sequence play vital roles in HIV-1 replication (Sarafianos et al., 2009). The dramatic effects of P/T sequence context on the removal efficiency of N[t]RTIs via phosphorolysis was surprising, since this effect could validate a compound being pharmacologically very effective or ineffective. There are only a very limited number of detailed published reports on this subject. One study showed significant alterations on ATP-mediated N[t]RTI removal efficiency from chain-terminated primers due to a single nucleotide substitution at different positions in a primer sequence originated from M13 bacteriophage DNA (Meyer et al., 2004). For our investigation, we utilized the aforementioned two distinct PPT and PBS sequences in order to explore the sequence dependency of TFV excision efficiency, where RT uses these HIV-1 genome sequences as substrates for viral DNA synthesis in a physiologically relevant setting. The influence of the sequence variation on AZT-MP excision has previously been examined using a PPT template sequence and two complementary primers where each primer binds at a different section of the same template (Marchand and Gotte, 2003). This study suggested that the efficiency of AZT-MP excision was directly correlated to the different preference of RT-DNA complex being at the nucleotide-binding site (N-site) or the priming site (P-site) for each primer sequence.

Here, we analyzed the removal of TFV from P/Ts derived from PPT and PBS sequences in the presence of ATP and PP_i as well as the inhibitory effects of EFV on the removal process while comparing both sequences side by side for the phosphorolysis reactions to understand the potential sequence related parameters that influence the removal efficiency. Our data indicate that the PPT sequence shows much more efficient phosphorolytic excision of TFV than PBS sequence, which suggests the sequence-derived DNA structure at the RT active site could promote interactions that modulate the productive TFV removal. This outcome also implies the evolutionary pressure for HIV-1 to preserve the PPT sequence because of its importance in viral survival. However, EFV compensates this potential resistance problem by forming a stable complex that would prevent TFV excision.

2. Materials and methods

2.1. Preparation and purification of HIV-1 RT

HIV-1 WT RT clone was generously provided by Stephen Hughes, Paul Boyer, and Andrea Ferris (Frederick Cancer Research and Development Center, Frederick, MD). C-terminal hexahistidine-tagged (only for the p66 subunit) heterodimeric p66/p51 reverse transcriptase was purified as previously described (Kerr and Anderson, 1997). Protein active site concentration was determined by pre-steady-state burst experiments as previously described (Ray et al., 2003).

2.2. Nucleoside triphosphates, and chemicals

All natural dNTPs, ATP, 2′,3′-dideoxythymidine triphosphate (ddTTP), and inorganic pyrophosphate (PP_i) were purchased from Sigma & Aldrich (St. Louis, MO) unless indicated otherwise. Tenofovir diphosphate (TFV-DP) was kindly provided by Dr. Michael D. Miller (Gilead Sciences, Inc., Foster City, CA). EFV was purchased from Toronto Research Chemicals Inc. (North York, Ontario, Canada) and diluted in dimethyl sulfoxide (DMSO). All nucleoside triphosphates were treated with thermostable pyrophosphatase (New England Biolabs, Beverly, MA) to degrade any contaminating pyrophosphate according to the manufacturer's protocol. The

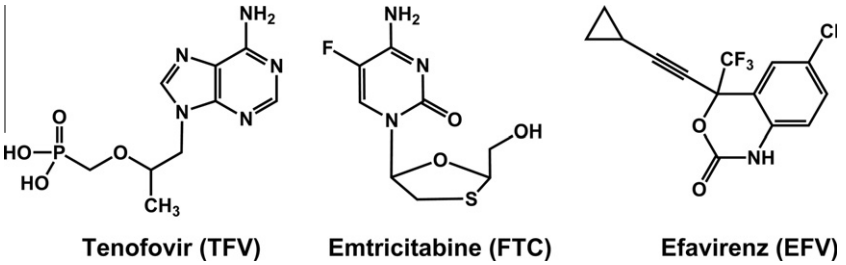

Fig. 1. Chemical structures of tenofovir, emtricitabine, and efavirenz.

nucleotides were purified by filtration through a 10-kDa-cutoff Microcon filter (Millipore, Billerica, MA).

2.3. Oligonucleotides

All of the DNA oligonucleotides with the following sequences were purchased from Integrated DNA Technologies (Coraville, IA) and further purified using 20% polyacrylamide denaturing gel electrophoresis. The sequences of all DNA primers and templates used for incorporation and removal studies are: PPT_D17 primer (5′-TTAAAAGAAAAGGGGGG-3′); PBS_D21 primer (5′-TCAGGTCCCTGTTCGGGCGCC-3′); D57 template (5′-CGTTGGGAGTGAATTAGCCCTTCCAGTCCCCCCTTTTCTTTTAAAAAGTGGCTAAGA-3′); and D36 template (5′-TCTCTAGCAGTGGCGCCCGAACAGGGACCTGAAAGC-3′). TFV-DP was incorporated into PPT_D17 and PBS_D21 primers by HIV-1 WT RT and both TFV-terminated primers (PPT_D17-TFV and PBS_D21-TFV) were gel purified according to the previously reported methods (Johnson et al., 2001). PPT_D17, PBS_D21, PPT_D17-TFV and PBS_D21-TFV primers were 5′-^{32}P-labeled with T4 polynucleotide kinase (New England Biolabs, Beverly, MA) using [γ-^{32}P]ATP purchased from PerkinElmer Health Sciences, Inc. (Shelton, CT). The excess [γ-^{32}P]ATP was removed by passing the reaction mixture through a biospin column from Bio-Rad (Hercules, CA). Concentrations of the oligonucleotides were estimated by UV absorbance at 260 nm using calculated extinction coefficients. PPT_D17 and PPT_D17-TFV DNA primers, and D57 DNA template were annealed by adding 1:1.4 M ratio of purified primer to the corresponding template at 90 °C for 5 min, 55 °C for 10 min, and on ice for 10 min. Additionally, PBS_D21 and PBS_D21-TFV DNA primers, and D36 DNA template were annealed according to the same protocol described above. In order to confirm complete annealing, the annealed primer-templates were analyzed using 15% nondenaturing polyacrylamide gel electrophoresis. For TFV removal studies, PPT_D17-TFV/D57 and PBS_D21-TFV/D36 P/T combinations were used and in order to examine ATP incorporation, PPT_D17/D57 and PBS_D21/D36 P/T pairs were used.

2.4. ATP-mediated TFV removal assays from P/Ts derived from PPT and PBS sequences

ATP-mediated TFV removal was studied as described previously (Ray et al., 2003) by quantitating the disappearance of primer band at a physiologically relevant concentration of 3 mM ATP in single-turnover experiments. 250 nM WT RT and 50 nM chain-terminated P/T (PPT_D17-TFV/D57, PBS_D21-TFV/D36) were preincubated in reaction buffer consisting of 50 mM Tris–HCl, pH 7.8, 50 mM NaCl for 5 min at 37 °C. Reactions were initiated by the addition of equal volume of 10 mM $MgCl_2$ and ATP (3 mM) mixture into the RT-DNA prebound complex solution and performed at 37 °C. All concentrations represent final concentrations unless indicated otherwise, and the enzyme concentration is based on a pre-steady-state active site determination. The reactions were stopped at various time points (0–120 min for PPT_D17-TFV/D57 and 0–240 min for PBS_D21-TFV/D36) by adding 10 μl aliquots of the reaction mixture into a 50 μl sample loading buffer (98% deionized formamide/0.5 M EDTA mixture containing 1 mg/ml each of bromophenol blue and xylene cyanol). Samples were heat denatured for 5 min at 95 °C and separated on a 20% polyacrylamide-8 M urea sequencing gel. Products were visualized and quantitated using a Bio-Rad Molecular Imager FX. Data was analyzed using Quantity One (Bio-Rad Laboratories, Inc., Hercules, CA).

The effect of next complementary nucleotide on ATP-mediated TFV removal was investigated by adding various concentrations (5, 10, and 50 μM) of dCTP, the next complementary nucleotide, to the reaction mixture. The experiments were repeated three times, and representative images are shown in Supplementary Fig. 1.

2.5. ATP-mediated TFV excision combined with the rescue of DNA synthesis experiments

Chain-terminated PPT_D17-TFV/D57 or PBS_D21-TFV/D36 (50 nM) was incubated with 250 nM WT RT in reaction buffer containing 50 mM Tris–HCl, pH 7.8, 50 mM NaCl at 37 °C for 5 min. In order to initiate the TFV excision and subsequent rescue of DNA synthesis, a mixture consisting of excess amount of dATP (100 μM) to prevent reincorporation of the excised TFV product, 10 μM dCTP, 100 μM ddTTP, and 10 mM $MgCl_2$ with 3 mM ATP as a pyrophosphate donor for the excision reaction were added (all concentrations represent final concentrations). Reactions were performed at 37 °C and stopped at different time points (0–240 min) by removing 10 μl aliquots of reaction mixture into a 50 μl of sample loading buffer. All samples were separated, visualized and analyzed as described above.

2.6. Pre-steady state single-turnover experiments for ATP incorporation

Rapid chemical quench experiments were performed with a KinTek Instruments model RQF-3 rapid quench-flow apparatus as described previously (Kati et al., 1992; Feng and Anderson, 1999). A pre-steady-state kinetic analysis was used to examine the incorporation of ATP into PBS_D21/D36, and PPT_D17/D57 P/Ts. Single-turnover experiments were exploited to analyze the rates of incorporation less than 2 s^{-1}. The reactions were carried out by rapid mixing of a solution containing the preincubated complex of 250 nM WT RT and 50 nM 5′-labeled P/T with a solution of 10 mM $MgCl_2$ and varying concentrations of ATP in the presence of 50 mM Tris–HCl, pH 7.8, 50 mM NaCl at 37 °C. The reaction was quenched by the addition of excess 0.5 M EDTA. Samples were diluted in formamide buffer containing 1 mg/ml each of bromophenol blue and xylene cyanol. All samples were separated and visualized as described above.

2.7. PP_i-mediated TFV excision experiments in the presence of efavirenz

PP_i-mediated TFV removal was studied by quantifying the disappearance of primer band in single-turnover experiments as described previously (Ray et al., 2003). Reactions were performed at 37 °C and initiated by the addition of equal volume of 10 mM $MgCl_2$ and 125 μM PP_i (physiologically relevant concentration (Barshop et al., 1991) mixture into the RT-DNA (250–50 nM) prebound complex in reaction buffer solution (all concentrations represent final concentrations). The reactions were stopped at various time points by adding 10 μl aliquots of the reaction mixture into a 50 μl sample loading buffer. All samples were separated, visualized and analyzed as described above.

In order to determine the IC_{50} value of EFV for the PP_i-mediated TFV excision reaction, 250 nM WT RT was incubated with 50 nM chain-terminated PPT_D17-TFV/D57 or PBS_D21-TFV/D36 P/T in 50 mM Tris–HCl, pH 7.8, 50 mM NaCl for 10 min on ice, and then varying concentrations of EFV (0–500 nM) was added which was incubated for an additional 10 min on ice. DMSO was used as a control for the removal experiments lacking EFV (representing less than 2% of total reaction mixture). Reactions were initiated by the addition of 125 μM PP_i and 10 mM $MgCl_2$ and performed at 37 °C using time course experiments. All time points (10 μl aliquots of reaction mixture) were quenched with 50 μl sample loading buffer. Samples were heat denatured for 5 min at 95 °C and separated on a 20% polyacrylamide-8 M urea gel. Reaction products were visualized and analyzed as described above.

2.8. Data analysis

Data were fitted by nonlinear regression using the program KaleidaGraph version 4.02 (Synergy Software, Reading, PA). Single-turnover incorporation and removal experiments were fitted to single-exponential equations: $[\text{product}] = A[1 - \exp(-k_{obsd}t)]$, where A represents the amplitude of product formation and k_{obsd} is the observed rate at a specific substrate concentration. The dissociation constant (K_d) of the ATP binding to the RT-DNA complex was calculated by fitting the observed rate constants at different concentrations of ATP to the following hyperbolic equation: $k_{obsd} = (k_{pol}[ATP])/(K_d + [ATP])$, where k_{pol} is the maximum rate of ATP incorporation, and K_d is the equilibrium dissociation constant for the productive interaction of ATP with RT–DNA complex. To determine the inhibitory concentration (IC_{50}) of EFV that decrease the efficiency of TFV excision by 50%, hyperbolic curves were fitted to the observed rate of PP_i-mediated TFV removal (k_{rem}) versus increasing concentrations of EFV from the generated pyrophosphorolysis data. Brackets denote concentration and reported errors represent the deviation of points from the curve fit generated by KaleidaGraph.

3. Results

3.1. ATP-mediated TFV removal assays from P/Ts derived from PPT and PBS sequences

In order to determine the significance of sequence context on the TFV excision efficiency, studies were carried out examining the two distinct viral sequences terminated with TFV as DNA:DNA P/T pairs; PPT_D17-TFV/D57 and PBS_D21-TFV/D36. All removal reactions were conducted at 3 mM ATP using WT RT. Our initial studies with the TFV terminated PPT sequence was somewhat surprising. For the case of PPT_D17-TFV/D57 P/T, as opposed to observing a TFV excised nucleotide band (marked as position n − 1 in Fig. 2B), we observed formation of a product band over time that migrates in close proximity to the labeled PPT_D17-TFV primer (marked as position n in Fig. 2B) while the primer band was disappearing. This would have arisen from TFV removal and ATP incorporation. This newly formed band is assigned as AMP incorporated PPT_D17 primer (PPT_D17-AMP), which also runs around the same range of an 18-mer on the gel. In order to verify the migration patterns, AMP and TFV incorporated PPT_D17 primers were prepared, and annealed to D57 template and run individually along with a 1:1 mixture of both oligonucleotides next to each other (Fig. 2C). An isolated migration distance was clearly observed between the PPT_D17-AMP and PPT_D17-TFV (Fig. 2C, lanes 2 and 3) primers alone, and as a mixture of 1:1 ratio both primers were staggered from one another reflecting the different electrophoretic migration pattern (Fig. 2C, lane 4). Besides the PPT_D17-AMP band, an additional second product band (marked as position n + 1) appeared at longer reaction time points around the length of a 19-mer. This band corresponds to a consecutive misincorporation of the ribonucleotide ATP molecule across a G in the template and indicated as PPT_D17-2AMP in Fig. 2B. The decrease in PPT_D17-TFV primer concentration was quantitated by phosphor imaging and the observed rate of ATP-mediated TFV removal (k_{rem}) was determined as a function of reaction time (Fig. 2D). The data was fitted to single exponential decay and k_{rem} value was determined to be $0.0085 \pm 0.0007\ s^{-1}$.

For the case of PBS_D21-TFV/D36 P/T, no apparent separation was observed between the TFV-terminated primer and the AMP incorporated product band compared to that observed with PPT_D17-TFV/D57 P/T. However, the labeled PBS_D21-TFV primer band presented a probable vertical expansion starting from the 60 min reaction time point until the 240 min time point compare to the earlier time points as shown in Fig. 3B, which could be explained as a mixture of newly formed PBS_D21-AMP and the remaining PBS_D21-TFV primer bands as we have seen in the PPT sequence. Moreover, the same kind of secondary product band corresponding to an A:G misincorporation (PBS_D21-2AMP) was formed at longer time points, yet vaguely visible (Fig. 3B). Further, a similar type of gel migration analysis was performed using PBS_D21-AMP and PBS_D21-TFV primers and the assay illustrated a minor separation in migration distance between the two primers alone, but the 1:1 mixture of both primers co-migrated as a single band without any detectable partition (Fig. 3C). As a result, the absence of a gap between the TFV- and ATP-terminated PBS_D21 primer bands hinders the precise quantification of the TFV excision. Therefore, no k_{rem} value was determined for the ATP-mediated TFV removal for PBS_D21-TFV/D36 P/T. However, comparing the ratio between the labeled TFV-terminated primer bands and the synthesized overall product bands over the reaction time course suggested that the removal of TFV from PPT_D17-TFV/D57 P/T was much more efficient than PBS_D21-TFV/D36 P/T in the presence of 3 mM ATP.

In parallel to the kinetic characterization of ATP-mediated TFV removal with PPT and PBS P/Ts, we also evaluated the effects of the next complementary nucleotide (dCTP) on the overall TFV excision efficiency (Supplementary Fig. 1). The data showed no significant changes on the efficiency of TFV excision at the concentrations of 5 and 10 μM dCTP in comparison to only ATP, yet 50 μM dCTP significantly reduced the removal efficiency of TFV due to the more favorable dead-end complex (DEC) formation, which is in agreement with a previous study by Marchand et al. (2007).

3.2. ATP-mediated TFV excision combined with the rescue of DNA synthesis experiments

To facilitate the quantification of ATP-mediated TFV removal efficiency for both P/Ts, another indirect approach that combines ATP-dependent excision reaction with the subsequent rescue of DNA synthesis was utilized through time course experiments using PPT_D17-TFV/D57 and PBS_D21-TFV/D36. In this method, besides 3 mM ATP (pyrophosphate donor), 100 μM dATP (the correct nucleotide for position n), 10 μM dCTP (a physiologically relevant concentration of the next complementary nucleotide for position n + 1), and 100 μM ddTTP (a dideoxy-nucleotide derivative as a chain terminator that base pairs with position n + 2) were added to the WT RT–DNA binary complex to generate an extended product band that could be distinguishable from the TFV blocked DNA primer upon excision (Fig. 4A). We found an 80% yield for the rescued DNA synthesis utilizing PPT_D17-TFV/D57, while PBS_D21-TFV/D36 showed only a 10% product yield (Fig. 4B). In summary, our findings in this setup confirm the results from the previous ATP-mediated excision assay suggesting that PBS sequence accommodates ATP-mediated TFV removal reaction much less proficiently than PPT sequence.

3.3. Incorporation of ATP into PPT and PPS sequence primers by WT RT

As a follow-up experiment, we determined the incorporation efficiency of ATP as an incoming nucleotide that is complementary to the template base, T, in both unblocked PPT_D17/D57 and PBS_D21/D36 P/Ts. This assay would facilitate a better understanding of the obtained 8-fold difference in the efficiency of TFV removal from the DNA rescue experiments between PPT and PBS sequences. Single-turnover incorporation experiments were carried out at varying concentrations of ATP where the PPT_D17/D57 and PBS_D21/D36 P/T sequences to determine the observed

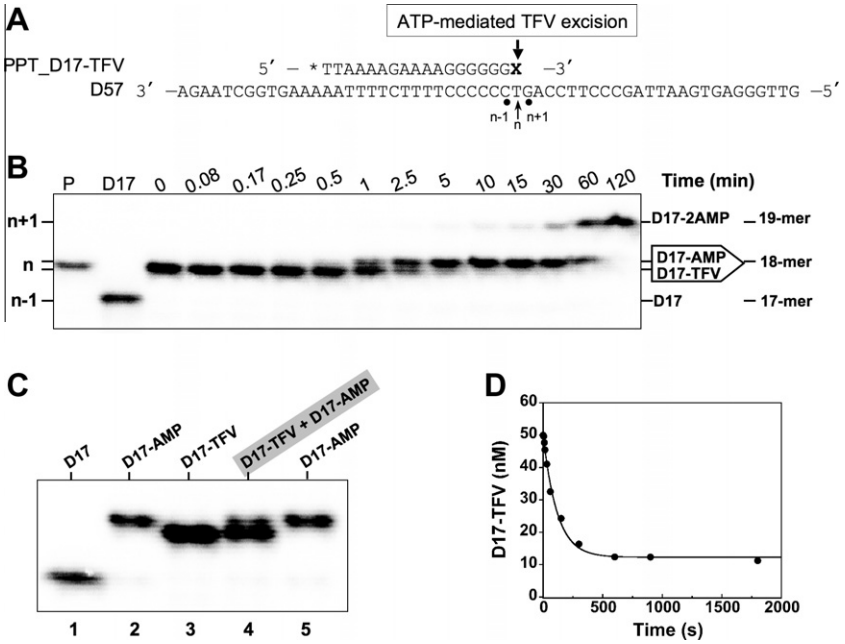

Fig. 2. ATP-mediated TFV excision from PPT_D17-TFV/D57 P/T by WT RT. (A) The sequence of PPT_D17/D57 chain terminated with TFV-DP (shown as X in the primer sequence). (B) ATP-mediated excision reactions were monitored in time course experiments using radiolabeled PPT_D17-TFV primer (lane P). The excision reactions were initiated by the addition of 3 mM ATP and stopped at the indicated time points. All samples were analyzed in denaturing 20% polyacrylamide gels. The D17 primer is indicated as 17-mer, the D17-TFV and the AMP incorporated (D17-AMP) primers are indicated as 18-mer, and the respective extended product (D17–2AMP) is indicated as 19-mer on the gel. (C) Electrophoretic migration distances of D17 (lane 1), D17-AMP (lanes 2 and 5), D17-TFV (lane 3), and 1:1 mixture of D17-TFV and D17-AMP (lane 4). (D) Rate of removal of the terminal TFV by 3 mM ATP from PPT_D17-TFV/D57.

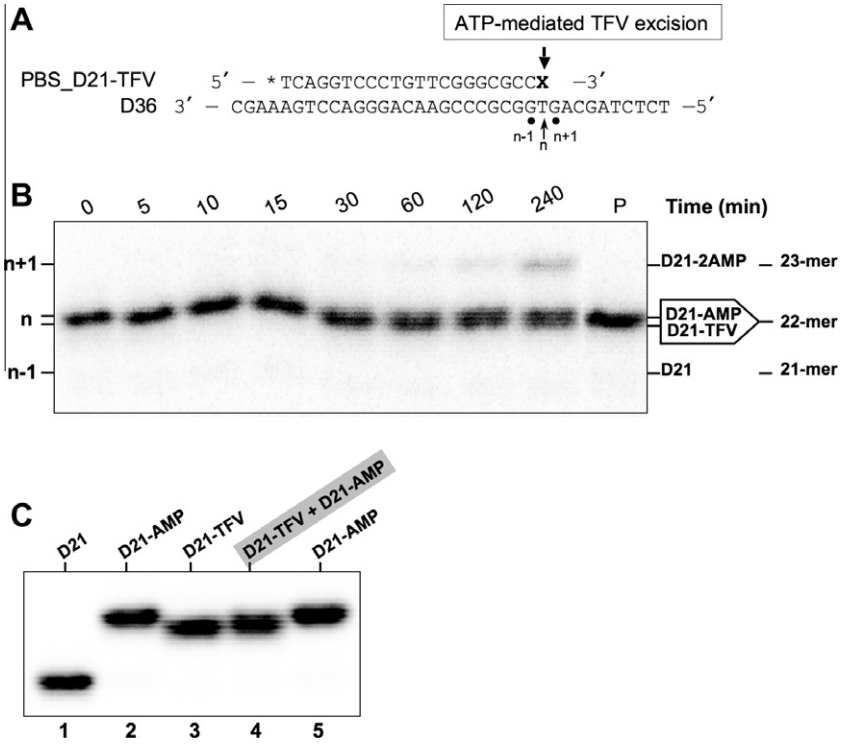

Fig. 3. ATP-mediated TFV excision from PBS_D21-TFV/D36 P/T by WT RT. (A) The sequence of PBS_D21/D36 chain terminated with TFV-DP (shown as X in the primer sequence). (B) ATP-mediated excision reactions were monitored in time course experiments using radiolabeled PBS_D21-TFV primer (lane P). The excision reactions were initiated by the addition of 3 mM ATP and stopped at the indicated time points. All samples were analyzed in denaturing 20% polyacrylamide gels. The D21-TFV and the AMP incorporated (D21-AMP) primers are indicated as 22-mer, and the respective extended product (D21-2AMP) is indicated as 23-mer on the gel. (C) Electrophoretic migration distances of D21 (lane 1), D21-AMP (lanes 2 and 5), D21-TFV (lane 3), and 1:1 mixture of D21-TFV and D21-AMP (lane 4).

rates of ATP incorporation (k_{obsd}) derived from plotting the elongated product concentration against reaction time (Fig. 5A and C). For each P/T, by plotting the values of calculated k_{obsd} against ATP concentration and fitting to a hyperbolic curve, the maximum

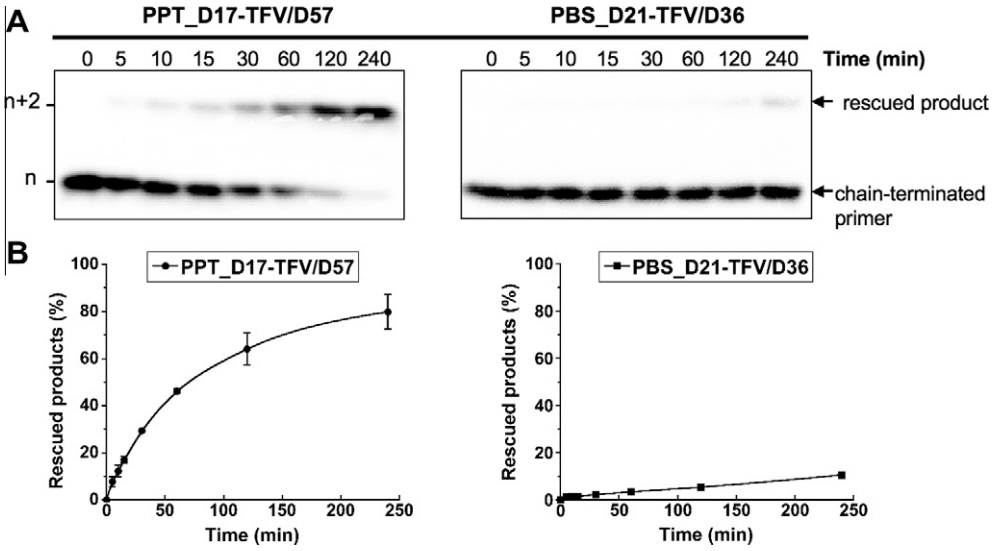

Fig. 4. Comparison of ATP-mediated excision efficiency of TFV from PPT and PBS P/Ts via DNA synthesis rescue experiments. (A) TFV terminated PPT_D17/D57 and PBS_D21/D36 P/Ts were mixed individually with 3 mM ATP and a mixture of 100 μM dATP, 10 μM dCTP, and 100 μM ddTTP to generate a rescued product band (n + 2) which is easy to distinguish from the chain-terminated primer (n) and reflects the removal efficiency. Reactions were stopped at the indicated time points and analyzed in denaturing 20% polyacrylamide gels. (B) Graphical representation of the average of three independent experiments ± standard deviations. Representative images are shown in panel (A). The rescued product yield is 80% for PPT_D17-TFV/D57 and 10.5% for PBS_D21-TFV/D36 at 240 min reaction time.

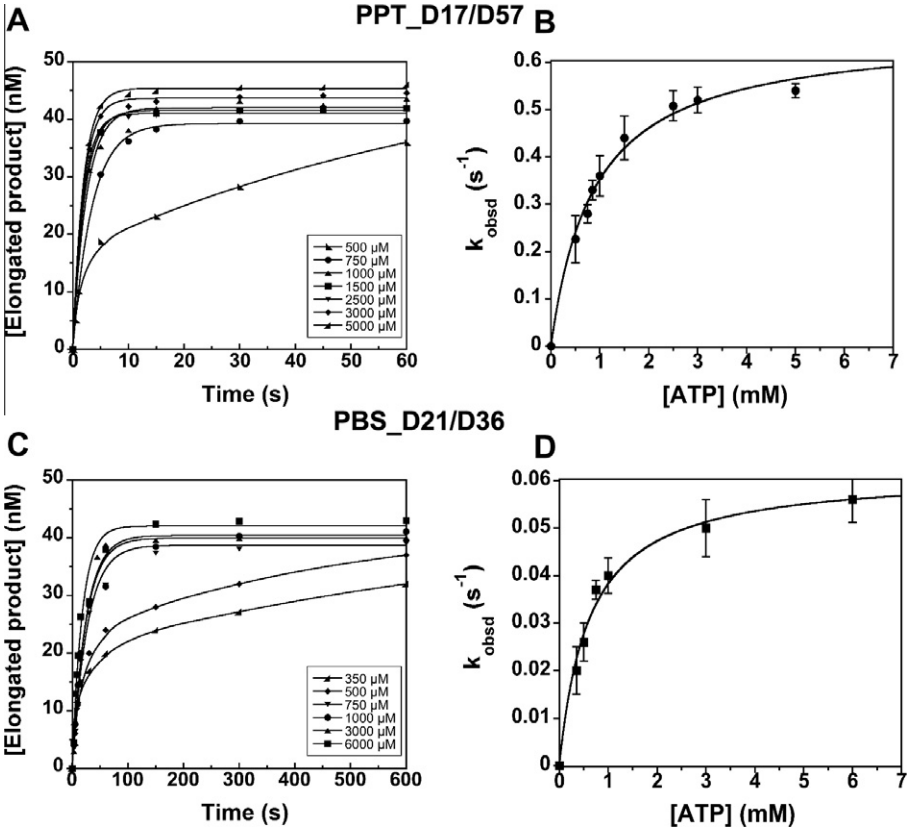

Fig. 5. The dependence of the observed rate of ATP incorporation on P/T sequences. (A) Pre-steady-state single-turnover kinetics of incorporation of ATP into PPT_D17/D57 P/T by WT RT were measured by mixing a preincubated WT RT (250 nM) and P/T (50 nM) with the various concentrations of ATP shown in the inlet and $MgCl_2$ (10 mM), which all concentrations are final after mixing. All the observed rate (k_{obsd}) values were calculated from plotting elongated product concentration against reaction time points. (B) All k_{obs} values were plotted against ATP concentration to generate K_d curves for PPT_D17/D57 P/T. The hyperbolic fit to the corresponding data gives a maximum rate of incorporation (k_{pol}) of 0.67 ± 0.02 s^{-1} and an equilibrium binding constant (K_d) of 887 ± 94 μM for PPT_D17/D57 (●) in graph (B). (C) Pre-steady-state single-turnover kinetics of incorporation of ATP into PBS_D21/D36 DNA P/T by WT RT were measured using various concentrations of ATP shown in the inlet and all k_{obs} values were calculated as mentioned above. All the k_{obs} values were plotted against ATP concentration to generate K_d curves for PBS_D21/D36 P/T. (D) The hyperbolic fit to the PBS_D21/D36 (■) data gives a k_{pol} of 0.062 ± 0.002 s^{-1} and K_d of 615 ± 75 μM for in graph (D).

rate of ATP incorporation (k_{pol}) and the binding constant for ATP (K_d) were determined (Fig. 5B and D and summarized in Table 1). As expected, ATP showed weak binding interactions with WT RT in the range of high-micromolar K_d values of 887 and 615 μM for PPT and PBS sequence primers, respectively. The efficiency of ATP incorporation (k_{pol}/K_d) was calculated to be 8-fold more efficient for PPT_D17/D57 in comparison to PBS_D21/D36, which was mostly affected by k_{pol} values (Table 1). Comparison of the incorporation efficiencies of ATP illustrates that the sequence context can modulate the incorporation rates much more than the binding constants.

3.4. PP_i-mediated TFV excision and the inhibitory effects of EFV on this reaction

Inorganic pyrophosphate was utilized due to the ability of visualization of the TFV excised products thus evaluating the kinetic parameters for removal efficiency of TFV from both P/T sequences. Table 2 summarizes the rate of TFV removal (k_{phys}) at physiological concentrations of 125 μM PP_i and 3 mM ATP using both P/Ts. In studies comparing PP_i-mediated TFV removal by WT RT utilizing PPT_D17-TFV/D57 and PBS_D21-TFV/D36 P/Ts, the kinetic data showed that the removal rate of TFV from PPT sequence derived P/T was 21-fold faster than the one derived from PBS sequence. Moreover, we found that PP_i-mediated TFV removal is 54-fold faster than the ATP-mediated removal using the detected values for PPT_D17-TFV/D57 P/T. The same comparison could not be done for PBS_D21-TFV/D36 since the ATP-mediated TFV removal yielded inseparable product bands on the sequencing gel. We also investigated the synergistic inhibitory effect of EFV and TFV at the enzymatic level through the addition of various concentrations of EFV into the PP_i-mediated TFV removal reactions (Fig. 6 and Table 3). These experimental data reveal an inhibitory effect on TFV removal rate at increasing concentrations of EFV using both P/Ts. The IC_{50} values for EFV were 51 and 35 nM for PPT_D17-TFV/D57 and PBS_D21-TFV/D36, respectively. We also calculated the maximal PP_i-mediated TFV removal rate (k_{rem}) values for each primer by fitting all the observed removal rates against varying concentrations of EFV (Table 3).

4. Discussion

N[t]RTI excision from the 3′ end of a chain-terminated DNA primer through pyrophosphorolysis reaction is one of the common resistance mechanisms that HIV-1 utilizes successfully (Menendez-Arias, 2010). To our surprise, early research on the efficiency of TFV removal showed a variety of confusing results derived from their observations, which could be due to the different experimental conditions and methods for the excision assays. For example, some studies monitored the ATP- and PP_i-mediated TFV excision directly by quantifying the overall ratio between the unblocked primer and the remaining chain-terminated primer after TFV removal reaction from DNA:RNA primer-template sequences using WT RT, which resulted in less than 5% and approximately 10% TFV removal in the presence of ATP and PP_i, respectively (Naeger et al., 2001, 2002; White et al., 2002). However, other studies utilized an indirect approach that extends the primer by either RT or other polymerases after TFV removal with WT RT and significantly higher percentages of TFV removal were observed using DNA:DNA primer-template sequences in the presence of ATP and PP_i (White et al., 2004; Boyer et al., 2004; Marchand et al., 2007). Another explanation for the differing outcomes could be the choice of primer-template sequences, which could influence the efficiency of N[t]RTI excision. Although the role of primer-template sequence context has been explored through the substitutions within the same sequence space for N[t]RTI removal (Meyer et al., 2004), there are no reports, so far, about the side-by-side comparison of two physiologically important HIV-1 specific sequences, PPT and PBS, for excision studies. Therefore, we decided to analyze the phosphorolytic removal of TFV from PPT along with PBS, uncovering the effects of sequence context on the efficiency of TFV removal. Here, we evaluated ATP-mediated TFV excision reactions under direct and indirect approaches for both primers as mentioned above. Additionally, we investigated PP_i-mediated TFV excision reactions with a direct approach using both primers in the presence of varying concentrations of EFV to probe the synergy between TFV and EFV. These are two out of three components of the FDA approved combination drug; Atripla. Our findings illustrate that PPT sequence facilitates more favorable TFV removal as opposed to PBS sequence in ATP and PP_i-mediated TFV excision, and that EFV inhibits excision-proficient HIV-1 RT, which may contribute to the antiviral synergy with TFV.

First, we investigated the ATP-mediated TFV removal, and our *in vitro* results showed no presence of a produced n-1 nucleotide band for both PPT_D17-TFV/D57 and PBS_D21-TFV/D36 P/Ts, which corresponds to the expected TFV-excised primer size. In contrast, we only detected a product band formation that has been identified as an AMP-incorporated unblocked primer with a similar electrophoretic migration distance to the disappearing TFV-terminated primer band. Because separately electrophoresed, AMP-incorporated primer bands migrated slightly higher than TFV-terminated primer bands due to the molecular size and structural difference in AMP's ribose sugar portion versus TFV's acylic sugar moiety. This observation led us to predict that ATP-mediated TFV removal rate should be slow enough that while one ATP molecule unblocks the primer, another ATP molecule can subsequently serve as an incoming nucleotide for the excised primer since both AMP and TFV possess the same nucleobase moiety, and then rapidly gets incorporated to the primer by WT RT. Our results are illustrated in the scheme shown in Fig. 7A. To assess this interpretation, we conducted ATP incorporation experiments using PBS_D21/D36 and PPT_D17/D57 P/Ts. Indeed, we observed a 79-fold rate difference between the ATP-mediated removal rate of TFV from PPT_D17-TFV/D57 and the incorporation rate of ATP into PPT_D17/D57, which supports our hypothesis. We also believe that this phenomenon can be seen with other nucleoside/nucleotide analogs that possess adenosine nucleobase, such as adefovir (9-[2-(2-phosphoromethoxy)ethyl]adenine).

In the case of PBS_D21-TFV/D36 P/T, the ATP-mediated removal process was similar except that the excision rate could not be cal-

Table 1
Kinetic and equilibrium constants for binding and incorporation of ATP by WT RT using PPT and PBS DNA sequences.

Primer/template	k_{pol} (s^{-1})	K_d (μM)	k_{pol}/K_d ($\mu M^{-1}s^{-1} \times 10^{-4}$)
PPT_D17/D57	0.67 ± 0.02	887 ± 94	7.6
PBS_D21/D36	0.062 ± 0.002	615 ± 75	1.0

Table 2
Removal rates of TFV from PPT and PBS DNA templated primers by ATP- and PP_i-mediated removal.

Primer/template	Substrate	k_{phys} (s^{-1})[a]
PPT_D17-TFV/D57	PPi	0.49 ± 0.04
	ATP	0.009 ± 0.0007
PBS_D21-TFV/D36	PPi	0.023 ± 0.001
	ATP	ND[b]

[a] k_{phys} is the rate of removal at a physiological concentration of the appropriate pyrophosphate donor (125 μM PPi or 3 mM ATP).
[b] Not detectable.

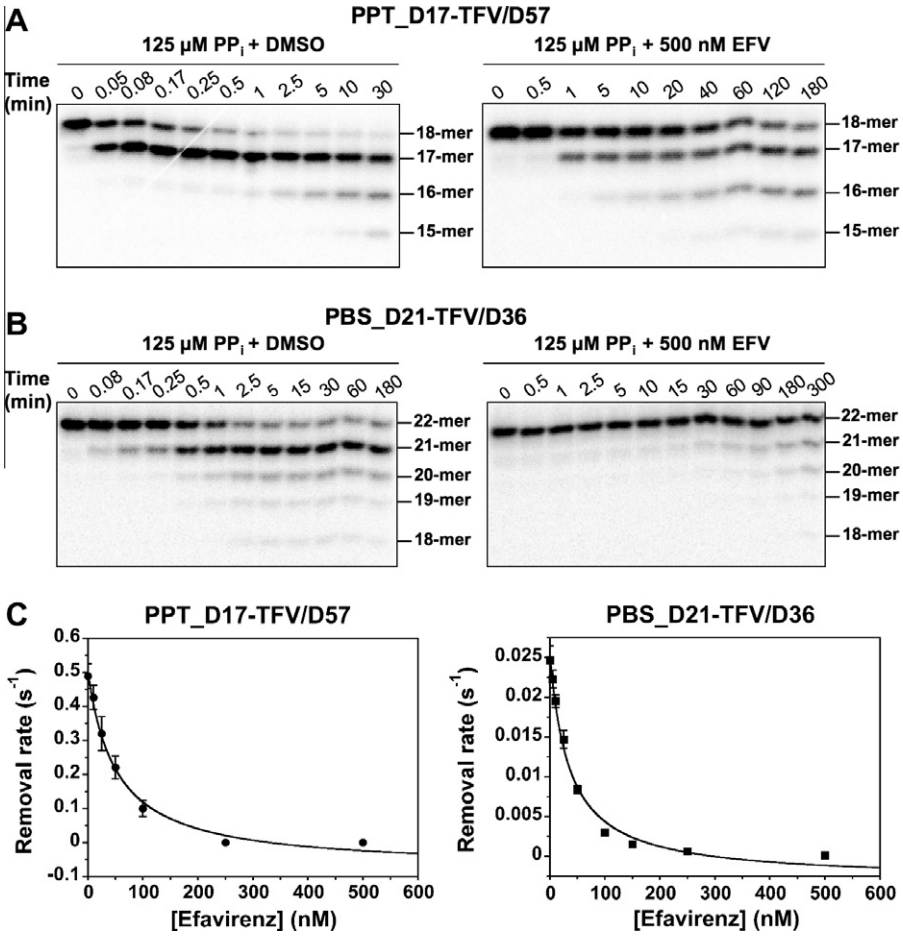

Fig. 6. Comparison of the PP_i-mediated TFV excision efficiency and the inhibitory effects of EFV on pyrophosphorolysis using PPT and PBS P/Ts. (A) PP_i-mediated TFV excision utilizing 125 μM PP_i in the absence and presence of EFV (500 nM) with PPT_D17-TFV/D57 and PBS_D21-TFV/D36 P/Ts (50 nM) catalyzed by WT RT (250 nM) at indicated time points. (B) Rates of removal of terminal TFV from both P/Ts were plotted against various EFV concentrations to generate the PP_i-mediated removal (k_{rem}) of 0.58 ± 0.03 s^{-1} and a half maximal inhibitory concentration (IC_{50}) of 51.3 ± 9.3 nM for PPT_D17/D57 (●) and k_{rem} of 0.028 ± 0.001 s^{-1} and IC_{50} of 35.0 ± 5.7 nM for PBS_D21/D36 (■).

culated due to the insufficient separation between the PBS_D21-TFV primer band and the produced PBS_D21-AMP product band. Nevertheless, we might deduce that TFV removal is much less efficient with the PBS_D21-TFV primer sequence when the overall product formation in excision reaction is compared to the one emerged from PPT_D17-TFV primer sequence. Furthermore, the efficiency of ATP incorporation for PBS_D21/D36 was 8-fold less in relation to PPT_D17/D57 and this can be mostly accounted for by the reduced incorporation rate since the binding affinity values for ATP are mostly unaffected with both primers.

Given the observed substantial differences in ATP-mediated TFV excision reactions in relation to the two primer sequences, we also conducted a primer rescue experiment for both primers to overcome the detection limitation especially for PBS primer. The outcome of this assay was consistent with our findings from the ATP-mediated TFV excision reactions. The PPT sequence showed an 8-fold enhancement in the excision efficiency over PBS sequence, linking the effectiveness of TFV removal reaction directly to the sequence variation of P/T. PPT and PBS sequences are similar in length but vary in composition, and our data clearly demonstrate the importance of the sequence-specific interactions between RT and duplex DNA for the N[t]RTI excision reactions. If one looks closely to both sequences, it is evident that PPT possesses more unique sequence motifs than PBS, which could play a critical role in HIV-1 RT-nucleic acid recognition and the possible effects on viral replication. PPT includes two $(A)_4$-tracts within the sequence and one $(G)_6$-tract at the 3′ terminal of the sequence. In the published literature, it has been shown that A-tract DNA characteristically has a B*-form helix comprising of a rigid structure with unusual narrow minor groove, which is different than canonical B-form structural features (Hud and Plavec, 2003; McConnell and Beveridge, 2001). Furthermore, a G-tract DNA transitions from B- to A-form helix and its helical axis bends toward the major groove leaving a wide minor groove, which is the opposite of an A-tract structure (Ng et al., 2000). In conclusion, the structural evidence illustrates that A-tract and G-tract DNA sequences have distinctive characteristics from other typical DNA sequences providing sequence directed axial curvatures in the helical structures, which could determine the binding specificity of a ligand or protein to these sequences. Thus, PPT sequences utilize these features efficiently to prevent the RNase H cleavage by RTs from all retroviruses including HIV-1 and maintain the precise cleavage

Table 3
Removal of chain-terminating TFV from PPT and PBS DNA templated primers by PP_i-dependent removal and the inhibitory potency values of EFV.

Primer/template	EFV	
	k_{rem} (s^{-1})[a]	IC_{50} (nM)[b]
PPT_D17-TFV/D57	0.58 ± 0.03	51.3 ± 9.3
PBS_D21-TFV/D36	0.028 ± 0.001	35.0 ± 5.7

[a] k_{rem} is the maximum rate of TFV removal.
[b] EFV concentration necessary to inhibit removal 50% at 125 μM PP_i.

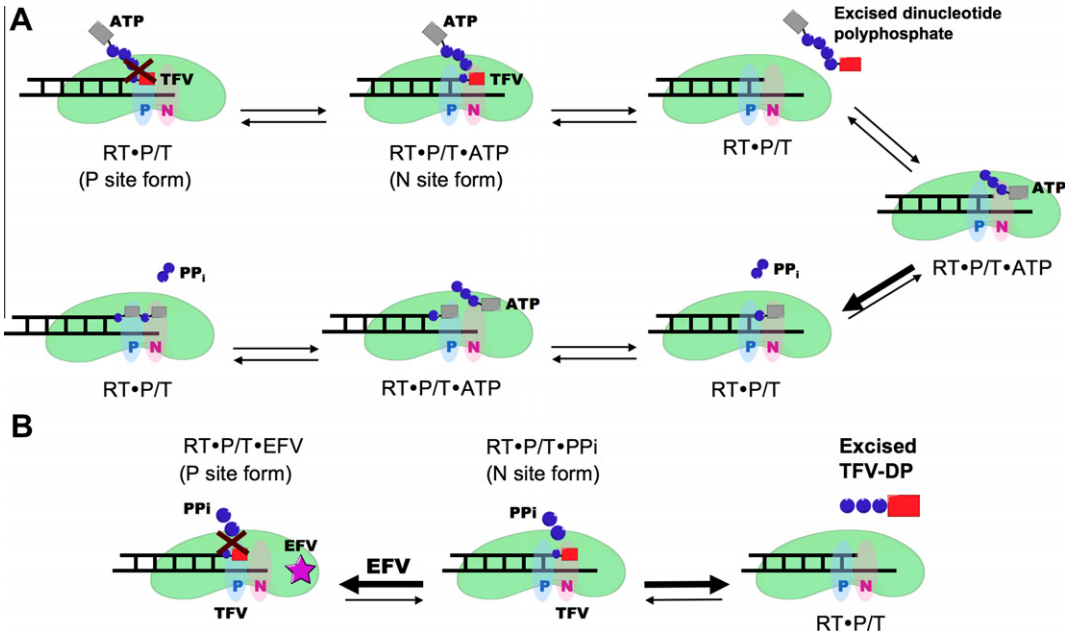

Fig. 7. Schematic representation of the TFV removal. (A) Illustration of the ATP-mediated TFV removal reaction steps using PPT_D17-TFV/D57 P/T. (B) Illustration of the inhibitory effects of EFV on pyrophosphorolytic removal of TFV for both sequences.

at the end of the PPT sequence that the generated primer initiates plus-strand DNA synthesis (Coffin et al., 1997). Several crystal structures of HIV-1 RT in complex with the DNA:RNA hybrid PPT duplex have been solved (Han et al., 1997; Sarafianos et al., 2001; Kopka et al., 2003). However, all of these reported X-ray structures were crystallized with PPT hybrid duplex only containing the two subsequent $(A)_4$-tract sequence while missing the $(G)_6$-tract part and showed structural evidence for the inability of the RNase H of RT to cleave this unique sequence where it resides at the RNase H site of RT. Unfortunately, there is no known RT structure solved with the $(G)_6$-tract situated at the polymerase site, which would complement our kinetic analysis and allow an understanding of the details of the connection between the sequence-dependent structure and RT function. We propose that the unique conformation of the $(G)_6$-tract segment with the incorporated TFV at the RT polymerase site could promote favorable binding modes of RT bound to the chain-terminated DNA duplex along with a pyrophosphate donor, such as ATP, for a competent TFV removal via phosphorolysis. It is also important to mention that there could be a strong evolutionary pressure to maintain the sequence of PPT since PPT is necessary for retroviral replication. This suggests that HIV-1 RT may remove any incorporated N[t]RTI at the PPT region more efficiently than any other part of the viral genomic sequence.

Combinations of an NNRTI with two N[t]RTIs, such as Atripla, are administered as a part of combination therapy in HIV-1 infected patients due to the confirmed synergistic effects at the enzymatic and cellular level. In order to hinder the efficient phosphorolytic removal of TFV, we utilized EFV in PP_i-mediated TFV excision using PPT_D17-TFV/D57 and PBS_D21-TFV/D36 P/Ts. We found that both primer/templates elicited diminishing TFV excision rate in correlation to the increasing amounts of EFV, which is in agreement with the previously published data on the observed synergism with the combination of EFV and several NRTIs (Basavapathruni et al., 2004; Cruchaga et al., 2005; Radzio and Sluis-Cremer, 2008; Feng et al., 2009). As anticipated, the k_{rem} value for PP_i-mediated TFV removal was 21-fold higher for PPT than PBS sequence, whereas an IC_{50} value for EFV was in a similar low nanomolar range. Based on our results, we suggest that upon binding of EFV at the allosteric NNRTI site of RT bound to TFV-terminated DNA duplex could induce conformational changes that might distort the binding network of the terminal TFV with the polymerase active site and/or the binding site for the nucleotide acceptor molecule (PP_i), leading to a non-productive binding orientation, hence diminished levels of TFV removal. Alone or in combination, any of the described effects would give rise to synergy in the overall observed RT inhibition. This conclusion is in accord with earlier studies that indicated two different conformational states of the terminal TFV were observed in the crystal structure of a TFV-terminated P/T bound to HIV-1 RT (Tuske et al., 2004). Consistent with earlier work (Feng et al., 2009), our results suggest that EFV binding to RT–P/T binary complex shifts the equilibrium towards the P site from the N site, where TFV is inaccessible for excision (Fig. 7B). As a result, EFV forms a stable complex that is similar to the conventional DEC formation through the next complementary nucleotide binding to the N site. Moreover, we propose that EFV could also induce long-range conformational changes in a region of RT occupied by the nucleotide acceptor molecules, such as ATP or PP_i and modulate their productive binding orientations resulting in diminished TFV excision as well. This type of effect was reported where different conformations of ATP molecule were observed for WT RT and AZT-resistant RT structures bound to the covalently attached AZTMP and ATP (dinucleoside tetraphosphate), in which mutations affect the ATP binding site and possible interactions with the residues surrounding the site (Tu et al., 2010).

In conclusion, the PPT sequence in the viral genome especially favors the excision of TFV over the PBS sequence whilst neutralizing the antiviral activity of TFV because of its unique helical structure at the active site of RT. Nevertheless, EFV obstructs the excision pathway that drives viral resistance and as a consequence enhances the desired antiviral efficacy against HIV-1. Taken together, the results of this study suggest that the effectiveness of ATP- or PP_i-mediated TFV excision is primarily dependent on the primer-template sequence that intertwines the molecular interactions with RT enzyme and the chemical entity of chain terminator. We believe that crystallographic analysis with the TFV terminated PPT and PBS P/T sequences bound to RT at the same position as we conducted our biochemical analysis will particularly enlighten the sequence-dependent N[t]RTI removal efficiency through providing structural evidence.

This study raises two interesting questions for further research: If we use DNA:RNA primer-template sequences to cover all the physiologically relevant possibilities, will there be a similar effect on TFV removal? Also, if TFV is combined with other clinically important NNRTIs, will there be a similar synergistic antiviral activity? Last year, FDA approved another fixed dose combination drug (Complera) containing FTC and TDF as two N[t]RTIs along with rilpivirine (also known as TMC278) as an NNRTI, which is the only difference compare to the Atripla coformulation (De Clercq, 2012). Studies are now under way to see if rilpivirine shares a similar kind of synergistic activity with TFV as efavirenz does, in addition to the potential effects of DNA versus RNA template sequences to uncover the molecular basis for the acquired outcomes. Finally, our data emphasizes the significance of the primer-template sequence framework for establishing the resistance profiles of the NRTIs that might have been overlooked previously. Future studies on assessing resistance of newly developed antiretroviral agents should consider utilizing various viral sequence frameworks rather than relying on one particular sequence. This strategy might offer a broader perspective for evaluating new drug candidates and potential drug resistance in more complex multidisciplinary clinical studies.

Acknowledgment

This work was supported by National Institutes of Health Grant GM49551 to K.S.A.

Appendix A. Supplementary data

Supplementary data associated with this article can be found, in the online version, at http://dx.doi.org/10.1016/j.antiviral.2012.z05.012.

References

Arion, D., Kaushik, N., McCormick, S., Borkow, G., Parniak, M.A., 1998. Phenotypic mechanism of HIV-1 resistance to 3′-azido-3′-deoxythymidine (AZT): increased polymerization processivity and enhanced sensitivity to pyrophosphate of the mutant viral reverse transcriptase. Biochemistry 37 (45), 15908–15917.

Barshop, B.A., Adamson, D.T., Vellom, D.C., Rosen, F., Epstein, B.L., Seegmiller, J.E., 1991. Luminescent immobilized enzyme test systems for inorganic pyrophosphate: assays using firefly luciferase and nicotinamide-mononucleotide adenylyl transferase or adenosine-5′-triphosphate sulfurylase. Anal. Biochem. 197 (1), 266–272.

Basavapathruni, A., Bailey, C.M., Anderson, K.S., 2004. Defining a molecular mechanism of synergy between nucleoside and nonnucleoside AIDS drugs. J. Biol. Chem. 279 (8), 6221–6224.

Boyer, P.L., Imamichi, T., Sarafianos, S.G., Arnold, E., Hughes, S.H., 2004. Effects of the Delta67 complex of mutations in human immunodeficiency virus type 1 reverse transcriptase on nucleoside analog excision. J. Virol. 78 (18), 9987–9997.

Coffin, J.M., Hughes, S.H., Varmus, H., 1997. Retroviruses. Cold Spring Harbor Laboratory Press, Cold Spring Harbor, NY.

Cruchaga, C., Odriozola, L., Andreola, M., Tarrago-Litvak, L., Martinez-Irujo, J.J., 2005. Inhibition of phosphorolysis catalyzed by HIV-1 reverse transcriptase is responsible for the synergy found in combinations of 3′-azido-3′-deoxythymidine with nonnucleoside inhibitors. Biochemistry 44 (9), 3535–3546.

Das, K., Lewi, P.J., Hughes, S.H., Arnold, E., 2005. Crystallography and the design of anti-AIDS drugs: conformational flexibility and positional adaptability are important in the design of non-nucleoside HIV-1 reverse transcriptase inhibitors. Prog. Biophys. Mol. Biol. 88 (2), 209–231.

Das, K., Martinez, S.E., Bauman, J.D., Arnold, E., 2012. HIV-1 reverse transcriptase complex with DNA and nevirapine reveals non-nucleoside inhibition mechanism. Nat. Struct. Mol. Biol. 19 (2), 253–259.

De Clercq, E., 2010. Antiretroviral drugs. Curr. Opin. Pharmacol. 10 (5), 507–515.

De Clercq, E., 2012. Where rilpivirine meets with tenofovir, the start of a new anti-HIV drug combination era. Biochem. Pharmacol..

De Clercq, E., 2009. Anti-HIV drugs: 25 compounds approved within 25 years after the discovery of HIV. Int. J. Antimicrob. Agents 33 (4), 307–320.

De Clercq, E., Neyts, J., 2009. Antiviral agents acting as DNA or RNA chain terminators. Handb. Exp. Pharmacol. (189), 53–84.

FDA notifications, 2009. FDA approves generic combination of efavirenz, lamivudine & tenofovir. In: AIDS Alert, vol. 24, p. 130.

Feng, J.Y., Anderson, K.S., 1999. Mechanistic studies comparing the incorporation of (+) and (−) isomers of 3TCTP by HIV-1 reverse transcriptase. Biochemistry 38 (1), 55–63.

Feng, J.Y., Ly, J.K., Myrick, F., Goodman, D., White, K.L., Svarovskaia, E.S., Borroto-Esoda, K., Miller, M.D., 2009. The triple combination of tenofovir, emtricitabine and efavirenz shows synergistic anti-HIV-1 activity in vitro: a mechanism of action study. Retrovirology 6, 44.

Hammer, S.M., Kessler, H.A., Saag, M.S., 1994. Issues in combination antiretroviral therapy: a review. J. Acquir. Immune Defic. Syndr. 7 (Suppl. 2), S24–S35, discussion S35–S37.

Han, G.W., Kopka, M.L., Cascio, D., Grzeskowiak, K., Dickerson, R.E., 1997. Structure of a DNA analog of the primer for HIV-1 RT second strand synthesis. J. Mol. Biol. 269 (5), 811–826.

Hud, N.V., Plavec, J., 2003. A unified model for the origin of DNA sequence-directed curvature. Biopolymers 69 (1), 144–158.

Johnson, A.A., Ray, A.S., Hanes, J., Suo, Z., Colacino, J.M., Anderson, K.S., Johnson, K.A., 2001. Toxicity of antiviral nucleoside analogs and the human mitochondrial DNA polymerase. J. Biol. Chem. 276 (44), 40847–40857.

Kati, W.M., Johnson, K.A., Jerva, L.F., Anderson, K.S., 1992. Mechanism and fidelity of HIV reverse transcriptase. J. Biol. Chem. 267 (36), 25988–25997.

Kerr, S.G., Anderson, K.S., 1997. RNA dependent DNA replication fidelity of HIV-1 reverse transcriptase: evidence of discrimination between DNA and RNA substrates. Biochemistry 36 (46), 14056–14063.

Killingley, B., Pozniak, A., 2007. The first once-daily single-tablet regimen for the treatment of HIV-infected patients. Drugs Today (Barc) 43 (7), 427–442.

Kopka, M.L., Lavelle, L., Han, G.W., Ng, H.L., Dickerson, R.E., 2003. An unusual sugar conformation in the structure of an RNA/DNA decamer of the polypurine tract may affect recognition by RNase H. J. Mol. Biol. 334 (4), 653–665.

Marchand, B., Gotte, M., 2003. Site-specific footprinting reveals differences in the translocation status of HIV-1 reverse transcriptase. Implications for polymerase translocation and drug resistance. J. Biol. Chem. 278 (37), 35362–35372.

Marchand, B., White, K.L., Ly, J.K., Margot, N.A., Wang, R., McDermott, M., Miller, M.D., Gotte, M., 2007. Effects of the translocation status of human immunodeficiency virus type 1 reverse transcriptase on the efficiency of excision of tenofovir. Antimicrob. Agents Chemother. 51 (8), 2911–2919.

McConnell, K.J., Beveridge, D.L., 2001. Molecular dynamics simulations of B′-DNA: sequence effects on A-tract-induced bending and flexibility. J. Mol. Biol. 314 (1), 23–40.

Menendez-Arias, L., 2010. Molecular basis of human immunodeficiency virus drug resistance: an update. Antiviral Res. 85 (1), 210–231.

Meyer, P.R., Matsuura, S.E., Mian, A.M., So, A.G., Scott, W.A., 1999. A mechanism of AZT resistance: an increase in nucleotide-dependent primer unblocking by mutant HIV-1 reverse transcriptase. Mol. Cell 4 (1), 35–43.

Meyer, P.R., Matsuura, S.E., So, A.G., Scott, W.A., 1998. Unblocking of chain-terminated primer by HIV-1 reverse transcriptase through a nucleotide-dependent mechanism. Proc. Natl. Acad. Sci. USA 95 (23), 13471–13476.

Meyer, P.R., Smith, A.J., Matsuura, S.E., Scott, W.A., 2004. Effects of primer-template sequence on ATP-dependent removal of chain-terminating nucleotide analogues by HIV-1 reverse transcriptase. J. Biol. Chem. 279 (44), 45389–45398.

Naeger, L.K., Margot, N.A., Miller, M.D., 2001. Tenofovir (PMPA) is less susceptible to pyrophosphorolysis and nucleotide-dependent chain-terminator removal than zidovudine or stavudine. Nucleosides, Nucleotides Nucleic Acids 20 (4–7), 635–639.

Naeger, L.K., Margot, N.A., Miller, M.D., 2002. ATP-dependent removal of nucleoside reverse transcriptase inhibitors by human immunodeficiency virus type 1 reverse transcriptase. Antimicrob. Agents Chemother. 46 (7), 2179–2184.

Ng, H.L., Kopka, M.L., Dickerson, R.E., 2000. The structure of a stable intermediate in the A ↔ B DNA helix transition. Proc. Natl. Acad. Sci. USA 97 (5), 2035–2039.

Radzio, J., Sluis-Cremer, N., 2008. Efavirenz accelerates HIV-1 reverse transcriptase ribonuclease H cleavage, leading to diminished zidovudine excision. Mol. Pharmacol. 73 (2), 601–606.

Ray, A.S., Murakami, E., Basavapathruni, A., Vaccaro, J.A., Ulrich, D., Chu, C.K., Schinazi, R.F., Anderson, K.S., 2003. Probing the molecular mechanisms of AZT drug resistance mediated by HIV-1 reverse transcriptase using a transient kinetic analysis. Biochemistry 42 (29), 8831–8841.

Sarafianos, S.G., Das, K., Tantillo, C., Clark Jr., A.D., Ding, J., Whitcomb, J.M., Boyer, P.L., Hughes, S.H., Arnold, E., 2001. Crystal structure of HIV-1 reverse transcriptase in complex with a polypurine tract RNA:DNA. EMBO J. 20 (6), 1449–1461.

Sarafianos, S.G., Marchand, B., Das, K., Himmel, D.M., Parniak, M.A., Hughes, S.H., Arnold, E., 2009. Structure and function of HIV-1 reverse transcriptase: molecular mechanisms of polymerization and inhibition. J. Mol. Biol. 385 (3), 693–713.

Spence, R.A., Kati, W.M., Anderson, K.S., Johnson, K.A., 1995. Mechanism of inhibition of HIV-1 reverse transcriptase by nonnucleoside inhibitors. Science 267 (5200), 988–993.

Staszewski, S., Morales-Ramirez, J., Tashima, K.T., Rachlis, A., Skiest, D., Stanford, J., Stryker, R., Johnson, P., Labriola, D.F., Farina, D., Manion, D.J., Ruiz, N.M., 1999. Efavirenz plus zidovudine and lamivudine, efavirenz plus indinavir, and indinavir plus zidovudine and lamivudine in the treatment of HIV-1 infection in adults. Study 006 Team. N. Engl. J. Med. 341 (25), 1865–1873.

Tantillo, C., Ding, J., Jacobo-Molina, A., Nanni, R.G., Boyer, P.L., Hughes, S.H., Pauwels, R., Andries, K., Janssen, P.A., Arnold, E., 1994. Locations of anti-AIDS drug binding sites and resistance mutations in the three-dimensional structure of HIV-1 reverse transcriptase. Implications for mechanisms of drug inhibition and resistance. J. Mol. Biol. 243 (3), 369–387.

Tsibris, A.M., Hirsch, M.S., 2010. Antiretroviral therapy in the clinic. J. Virol. 84 (11), 5458–5464.

Tu, X., Das, K., Han, Q., Bauman, J.D., Clark Jr., A.D., Hou, X., Frenkel, Y.V., Gaffney, B.L., Jones, R.A., Boyer, P.L., Hughes, S.H., Sarafianos, S.G., Arnold, E., 2010. Structural basis of HIV-1 resistance to AZT by excision. Nat. Struct. Mol. Biol. 17 (10), 1202–1209.

Tuske, S., Sarafianos, S.G., Clark Jr., A.D., Ding, J., Naeger, L.K., White, K.L., Miller, M.D., Gibbs, C.S., Boyer, P.L., Clark, P., Wang, G., Gaffney, B.L., Jones, R.A., Jerina, D.M., Hughes, S.H., Arnold, E., 2004. Structures of HIV-1 RT-DNA complexes before and after incorporation of the anti-AIDS drug tenofovir. Nat. Struct. Mol. Biol. 11 (5), 469–474.

White, K.L., Chen, J.M., Margot, N.A., Wrin, T., Petropoulos, C.J., Naeger, L.K., Swaminathan, S., Miller, M.D., 2004. Molecular mechanisms of tenofovir resistance conferred by human immunodeficiency virus type 1 reverse transcriptase containing a diserine insertion after residue 69 and multiple thymidine analog-associated mutations. Antimicrob. Agents Chemother. 48 (3), 992–1003.

White, K.L., Margot, N.A., Wrin, T., Petropoulos, C.J., Miller, M.D., Naeger, L.K., 2002. Molecular mechanisms of resistance to human immunodeficiency virus type 1 with reverse transcriptase mutations K65R and K65R + M184V and their effects on enzyme function and viral replication capacity. Antimicrob. Agents Chemother. 46 (11), 3437–3446.

Zhan, P., Liu, X., Li, Z., Pannecouque, C., De Clercq, E., 2009. Design strategies of novel NNRTIs to overcome drug resistance. Curr. Med. Chem. 16 (29), 3903–3917.